Space Interferometry Mission Spacecraft Pointing Error Budgets

Allan Y. Lee[†],
Jeffrey W. Yu,
Peter B. Kahn, and
Richard L. Stoller

Jet Propulsion Laboratory,
California Institute of Technology

Preliminary error budgets for the pointing knowledge, control, and stability of the SIM spacecraft are constructed using the specifications of commercial off-the-shelf attitude determination sensors, attitude control actuators, and other spacecraft capabilities that have been demonstrated in past missions. Results obtained indicate that we can meet all the presently known spacecraft pointing requirements. A large number of derived requirements are generated from this study. Examples are specifications on attitude determination sensors, attitude control actuators, minimum settling time after a rest-to-rest spacecraft slew. Preliminary error budgets constructed in this study must be updated to reflect the changing spacecraft design and requirements.

[†]M.S. 230-104, 4800 Oak Grove Drive, Pasadena, CA 91109-8099, USA.

I. INTRODUCTION

In the year 2005, the National Aeronautics and Space Administration (NASA) Space Interferometry Mission (SIM) will send an interferometer into space to operate above the Earth's atmosphere. SIM will yield star positions 250 times more accurately and narrow-field imaging with four times finer resolution than the best currently available techniques. These goals are to be achieved via a technique called optical interferometry. A preliminary configuration design of the SIM spacecraft is depicted in Fig. 1 [1].

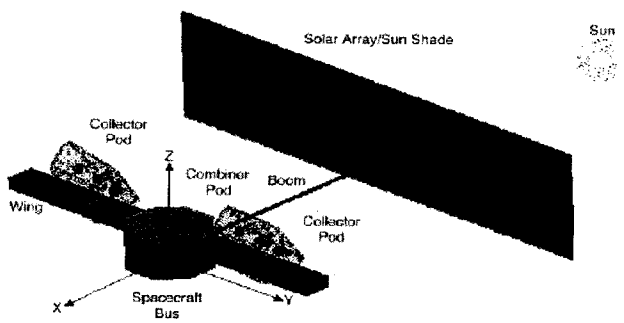

Fig. 1 A preliminary SIM configuration

A. Stellar Interferometer

An interferometer uses two telescopes (or collectors) on a common baseline to collect light from a target star. Because of SIM orientation, the star light wavefront will reach the telescopes at different times, making one light path to be shorter than the other. The operating principle of a Michelson stellar interferometer (in two dimensions) is illustrated in Fig. 2.

Astrometry determines the angle θ (in Fig. 2) between the target star and the interferometer baseline. This angle

can be found if we can determine the path-length difference (d in Fig. 2) and the baseline length between the two telescopes (|B|). To determine the path-length difference, one branch of the two light waves is "delayed" via an active optical delay line before it is "combined" with the other light wave (by a beam "combiner") to form an interference pattern. A bright fringe appears on a detector when the external and internal (that generated by the optical delay line) path-length differences are exactly the same. By making accurate measurements of both the internal path-length difference and the baseline length using a laser metrology system, the location of the star can be accurately determined ($\theta = \cos^{-1}[d/|B|]$). For further information on optical interferometry, see [2].

B. Science Objectives

Major science goals of the SIM mission include the following. For Astrometry in visible light (0.4 to 0.9 μm wavelength), SIM will measure star positions to an overall mission accuracy of better than 4 μsêc(1σ per axis) over wide angles (15° Field of View, FOV) and for 20th magnitude stars. For narrow angles (1° FOV) and for 12.5 magnitude stars, the mission accuracy requirement is 0.26 μsêc (1σ per axis). For imaging very small objects, or selected regions of larger objects, the SIM's imaging resolution goal is 10 mas (1 mas $=10^{-3}$ sêc). In support of the Terrestrial Planet Finder program, SIM will demonstrate a technique called interferometric nulling. Here, SIM's goal is to be able to reveal the properties of proto-planetary disks to within a few AU from the star, perhaps revealing structures in the disk attributable to a planetary system.

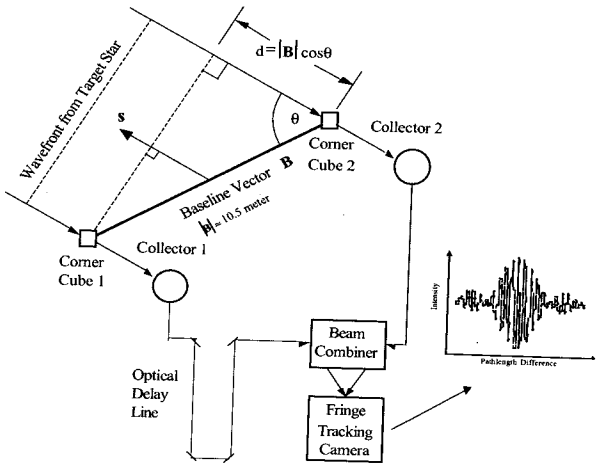

Fig. 2 Michelson stellar interferometer

C. Relation between Instrument and Spacecraft Pointing Control Systems

To "combine" two starlight beams together at the same physical location with the same optical phase, the interferometers rely on two classes of control loops: pointing control and path-length control loops.

The pointing control loop of an interferometer is responsible for tracking target stars. But before it can perform this function, the Attitude Control System (ACS) of the SIM spacecraft must be able to point the coarse acquisition camera of the interferometer with an accuracy that allows it to acquire these target stars. The required level of Spacecraft (S/C) pointing control requirement will be addressed in Section II. Once two coherent beams from a star are acquired, two similar pointing control loops will direct them onto a CCD (Charge Coupled Device) detector

in the focal plane of the Fringe Tracking Camera (FTC). Images captured on the FTC and high bandwidth fast steering mirrors (which are located in between the telescopes and the beam combiner) are then used in the pointing control loops to track the captured stars continuously in the presence of wide-band disturbances due to thermal and mechanical effects. Next, the path-length control loop is used to acquire and track the central fringe.

The path-length control loop of an interferometer is responsible for tracking the bright central fringe. But before it can perform this function, the attitude control system of the SIM spacecraft must provide the interferometer with estimates of both the central fringe position and the uncertainty of that position estimate. This information, to be provided by the on-board spacecraft attitude estimator, is used by the fringe acquisition algorithm to acquire the central fringe in finite time duration. Again, the required level of S/C pointing knowledge requirement will be discussed in Section II. Once the central fringe is captured, the path-length control loop will use low bandwidth stepper motors, medium bandwidth voice coils, and high bandwidth piezoelectric actuators to track the acquired central fringe.

In order to satisfy both the wide angle and narrow angle mission accuracy requirements, the SIM Instrument system must satisfy the following requirements (1σ per axis) [3]:

Pointing control accuracy	30 mas
Pathlength control accuracy	10 nm

Details of other measurement accuracy (e.g., the External metrology measurement accuracy) are given in Reference 4.

II. SPACECRAFT ARCHITECTURE AND POINTING REQUIREMENTS

A. Spacecraft Architecture

At the time this paper is being written, the SIM project is evaluating two architectures known as "SIM Classic" and "Son-of-SIM" (SOS). They differ chiefly in how they establish a common baseline for the guide and science interferometers, and in the relative complexity of their external metrology and pointing control system.

In the "SIM Classic" architecture, each of the three baselines is defined by a separate pair of corner cubes. As such, the External metrology system is more complex because it must process many measurements to identify small misalignments between the three baselines in addition to determining the distances between their end points. But the pointing system is simpler because it is not subject to a special constraint (described below) that must be satisfied in the case of the SOS architecture.

In the "SOS" architecture (cf. Fig. 1), two corner cubes define a common baseline that is shared by all three interferometers. The External metrology of the SOS architecture is simple because only one linear distance between two corner cubes has to be measured. However, the Instrument pointing control system is complex because each arm of the Instrument system must be articulated in

such a way that its field of regard always includes the appropriate corner cube in addition to the target star.

The spacecraft pointing error budgets constructed in this paper implicitly assumed the SOS architecture (cf. Fig. 1).

B. Definitions of Spacecraft Pointing Terminology

In this paper, the spacecraft on-board pointing knowledge error is defined to be the magnitude of the error vector between the actual pointing vector and the pointing vector estimated by the on-board attitude estimator. Similarly, the pointing control error is the magnitude of the error vector between the desired and actual S/C (spacecraft) pointing vectors. See Fig. 3.

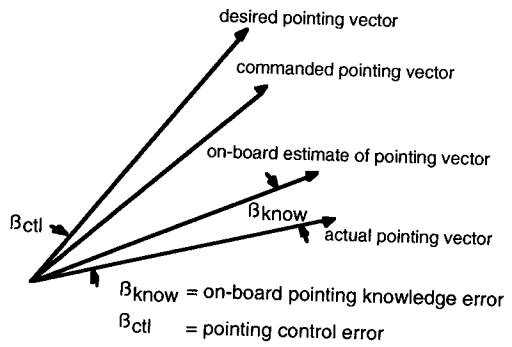

Fig 3 Spacecraft pointing vectors

A so-called "peak-to-peak" pointing stability metric is commonly used to specify the level of motion stability of either a S/C body-fixed axis or the line-of-sight (LOS) of an on-board instrument. One drawback of this pointing stability metric is that it uses only the two extrema points in the time history of the pointing vector that fall within a time window of interest. Another pointing stability metric that had been used in past missions is the Root-Mean-Squares (RMS) pointing stability metric (S_{rms}). If $B^2(f)$, in sec^2/Hz, denotes the power spectrum of the LOS angular excursion $\theta(t)$, then:

$$S^2_{rms} = \int_0^\infty B^2(f)\, df \qquad (1)$$

Here, f = frequency. S_{rms} is a simple way to measure motion stability. However, the degree to which disturbances at different frequencies contribute to jitters is also a function of the time window of interest, T, which is not considered in defining S_{rms}. In this paper, a "weighted" RMS pointing stability metric, S_{wrms}, first introduced by Lucke, Sirlin, and San Martin [4] is adopted. In the frequency domain, it is given by:

$$S^2_{wrms} = \int_0^\infty B^2(f) W_d(C)\, df, \qquad (2)$$

Here, $W_d(C) = 1\text{-}2(1\text{-}\cos C)/C^2$ and $C = 2\pi fT$. Fig. 4 depicts how the weighting function $W_d(C)$ varies with its argument C.

In Fig. 4, we note that $W_d > 0.5$ when $C \geq 2.78$. That is, for a time window T of 10 msec, disturbances at frequencies higher than $2.78/(2\pi \cdot 0.01) \approx 44.2$ Hz will have a greater impact on the spacecraft pointing stability than those below that frequency. In other word, the weighting function W_d is a high-pass filter with a "crossover" frequency near $2.78/(2\pi T) \approx 0.442/T$ Hz. See Section VI for a further discussion of this topic.

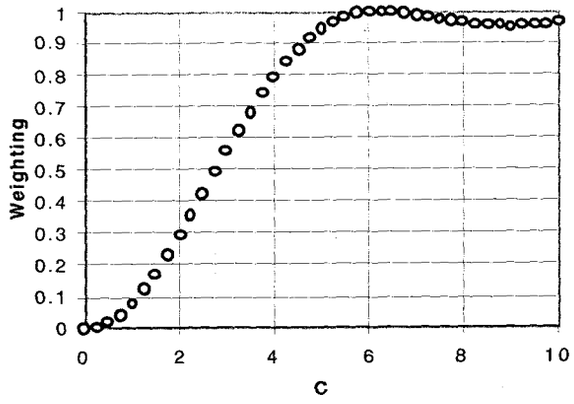

Fig. 4 The weighting function $W_d(C)$

C. SIM Coordinate Frames Definitions

Three coordinate frames are next defined in to better describe various SIM spacecraft (S/C) pointing requirements. The spacecraft mechanical frame C^{MECH} is depicted in Fig. 1. Nominally, the X-axis of the C^{MECH} frame is parallel to the nominal direction of the solar array boom. Its Y-axis is parallel to the common baseline of the interferometers, and the Z-axis completes a right-handed XYZ coordinate system. The origin of the C^{MECH} frame is at the center of the separation plane between the launch vehicle and the spacecraft, and the positive directions of the axes are indicated in Fig. 1.

The Attitude Control Subsystem (ACS) frame is denoted by C^{ACS}. As indicated in Fig. 5, the X and Z axes of the C^{ACS} frame lie in the plane of the Stellar Reference Unit's (SRU) footprint while its Y-axis is parallel to the SRU's bore-sight. The inertial attitudes of the C^{ACS} axes are to be estimated by an on-board attitude estimator, using measurements from both the SRU and Inertial Reference Units (IRUs). The spacecraft pointing requirements about both the X and Z axes of the C^{MECH} frame are more stringent than those about the Y axis. As such, we align the bore-sight axis of the SRU with the Y-axis of the C^{MECH} frame.

The coordinate frame with respect to which the spacecraft pointing requirements are levied is the SIM reference coordinate frame, C^{SIM}. The common baseline (B) shared by both the science and guide interferometers, called "physical baseline", is the Y-axis of the C^{SIM} frame. It joins the corner cubes located in the left and right collector pods. With reference to Fig. 5, let S denote the centerline vector of the science collector mirror field of regard (nominally, it lies within the +YZ plane of C^{MECH} frame, and is 20° away from the Z-axis). The X-axis of the C^{SIM} frame is parallel to the cross product of the B and S vectors, and the Z-axis of C^{SIM} frame completes a right-handed XYZ coordinate system. The vertex of the left corner cube (the one with a negative Y-axis coordinate in the C^{MECH} frame) is designated the origin of the SIM reference frame.

D. Preliminary Spacecraft Pointing Requirements

Preliminary SIM spacecraft pointing requirements include the following three components. First, on-board pointing knowledge requirements of 20 sêc, 3σ per X and Z axes, and 120 sêc, 3σ per Y axis. Secondly, pointing control requirements of 30 sêc, 3σ per X and Z axes, and 120 sêc, 3σ per Y axis. Lastly, pointing stability of 1.6 mas over a 0.01-second time window, 1σ per X and Z axes

(and none about the Y axis). Drivers behind these spacecraft pointing requirements are given next.

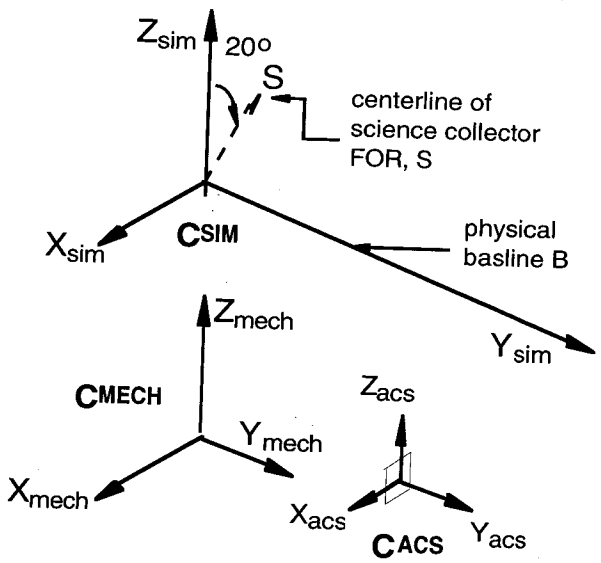

Fig. 5 SIM coordinate frames

The S/C pointing control requirements are driven by the need to ascertain that a selected guide star falls within the FOV of the coarse acquisition camera of the guide interferometer when it is commanded to point at that star. In the current SIM design, the FOV of the acquisition camera is 5 $\hat{\text{m}}\text{in}$.[4] If the S/C pointing control requirement is met, the guide star is guarantee to fall within the FOV of the acquisition camera.

The S/C on-board attitude knowledge requirements are driven by the need to successfully complete a guide star fringe acquisition within a finite time duration. A S/C attitude knowledge error of 20 $\hat{\text{sec}}$ corresponds to about 1 mm (3σ) in knowledge uncertainty in the central fringe position (20 $\hat{\text{sec}}\times 10$ m $\approx$ 1 mm). The number of fringe search steps, each 10 μm, that is required to complete a $\pm 4\sigma$ search is: $4\times 2\times(1/3 \text{ mm})/10\ \mu\text{m} \approx 267$ steps. With an integration time of 0.01 seconds for each search step, the worst-case total integration time is 2.67 seconds. Add to that the stepping time, the estimated time to complete a fringe acquisition is on the order of 4-5 s, which is an accepted acquisition time.

The spacecraft pointing stability requirement is driven by the need to maintain a high level of optical path-length stability over all 10-msec integration time steps during the fringe acquisition process. Good path-length stability leads to high signal-to-noise on the guide fringes, positively enabling fringe detection. An estimate of an acceptable level of path-length stability is 80 nano-meter (nm) (1σ).[4] Hence, the pointing stability of the spacecraft, about both the X and Z axes of the C^{SIM} frame, is 80×10^{-9} m/10 m $\approx$ 1.6 mas (1σ per X and Z axes) over 10-msec time windows.

III. SPACECRAFT ATTITUDE CONTROL SYSTEM

The stringent spacecraft pointing requirements described above are to be achieved via a well designed Attitude Control Subsystem (ACS) of the SIM spacecraft. Spacecraft's three-axis attitude is estimated using measurements from both the IRUs and the SRUs. To this end, the identities of stars captured by the star tracker are first established by an on-board star identification algorithm. The inertial attitudes of these identified stars,

given in an on-board star catalog, are then used to determine the inertial attitudes of the SRU axes. Via periodic in-flight calibrations between the SRU's axes (ACS frame) and other body-fixed vectors of interest (e.g., the radio frequency bore-sight of the High Gain Antenna (HGA), with residual calibration error on the order of fraction of a milli-radian), the inertial attitudes of these vectors are estimated.

Three Reaction Wheel Assemblies (RWAs) are used to control the S/C base-body. A fourth RWA is provided as a backup. The RWAs are also used to slew the S/C from one commanded attitude to another. With an Earth-trailing orbit, only solar radiation imparts a significant disturbance torque on the SIM spacecraft. The resultant angular momenta accumulated on these RWAs must then be unloaded using thrusters periodically.

The spacecraft ACS also responds to ground-commanded pointing of both the Solar Array/Sun Shield (SA/SS) and the High Gain Antenna (HGA). With reference to Fig. 1, the SA/SS is attached to the spacecraft base-body via a solar array boom. The relative orientation of the boom with respect to the base-body is to be controlled via a two degrees-of-freedom (dof) solar array drive mechanism (SADM). The attitude control subsystem also performs other engineering functions such as to detumble the S/C after the spacecraft-launch vehicle separation, and to maintain a safe-hold attitude in response to safing requests.

IV. ERROR SOURCES

The pointing performance of the SIM S/C is affected by several classes of error sources. They include the attitude determination error, star tracker bias error, residual errors after inflight calibrations, thermal distortions between inflight calibrations, slew-induced structural vibration, RWA controller error, RWA-induced structural vibration, S/C-solar array control interaction, thermal flutter, and S/C-instrument control interaction.

A. Attitude determination error

The ACS Attitude Estimator (ATE) is basically a Kalman-Bucy filter that uses measurements from a SRU and a set of IRUs. Inertial attitude updates are given by the SRU at intervals of ΔT seconds. In between these star measurement updates, the S/C attitude estimates are propagated using the IRU measurements.

The performance of the ATE can be estimated using an error covariance analysis. It provides an estimate of the ATE error due to both the rate white noise (angle random walk) and bias instability of the IRU, as well as the Noise Equivalent Angle (NEA) of the SRU.

When the S/C is quiescent, the attitude estimator error vector $\vec{e} = [e_x\ e_y\ e_z]^T$ and the IRU bias $\vec{b} = [b_x\ b_y\ b_z]^T$ are governed by the following equation: $\vec{x}_k = \Phi_{k-1}\ \vec{x}_{k-1} + \vec{w}_{k-1}$. Here, $\vec{x} = [\vec{e}^T\ \ \vec{b}^T]^T$ is the state vector of the ATE, and $\vec{w}$ is a zero-mean, white sequence with covariance Q_k. Q_k is given by $\Delta T \times [N_1 \cdot I_3\ O_3;\ O_3\ N_2 \cdot I_3]$,

where ΔT is the time duration between star measurement updates, and N_1 and N_2 denote the power spectral densities of the IRU rate white noise and bias instability, respectively. The state transition matrix Φ_{k-1} is a constant 6×6 matrix that is approximated by $I_6+\Delta T\times [O_3 \; -I_3; O_3 \; O_3]$.

The measurement equation is given by: $\vec{Z}_k = H_k \; \vec{X}_k + \vec{V}_k$, where $\vec{Z}$ is a 3×1 star measurement vector, H is a constant measurement matrix given by $[I_3 \; O_3]$, and $\vec{V}$ is a vector of zero-mean random noise with covariance R_k (due to the SRU's NEA). The propagation of the error covariance matrix of $\vec{X}$ is governed by the following set of equations:

$$P_k(-) = \Phi_{k-1} \; P_{k-1}(+) \; \Phi^T_{k-1} + Q_{k-1}$$

$$P_k(+) = [I_6 - K_k \; H_k] \; P_k(-) \qquad (3)$$

$$K_k = P_k(-) \; H^T_k \; \{ \; H_k \; P_k(-) \; H^T_k + R_k \; \}^{-1}$$

where $P_k(-)$ and $P_k(+)$ denote the error covariance matrices of the state vector computed immediately before and after the k^{th} star measurement update, and K_k denotes the Kalman-Bucy gain at time step k. Using these equations, we can compute the time propagation of the ATE errors about the three S/C axes. Error budgets given in Section V contain per-axis attitude determination errors that were computed using the following set of sensor specifications: ΔT = 1 second, $N_1 = 10^{-8}$ deg^2/hr, $N_2 = 10^{-3}$ deg^2/hr^3, and the NEAs of SRU are 1.5 and 25 (twist) sêc, 3σ per axis.

Sensor noise with a significant frequency content within the controller bandwidth looks like valid "command" to the control loop. Accordingly, the controller will generate control torque in order to cause the S/C attitude to follow these erroneous "commands." This results in undesired S/C motion. To estimate the impact of both the SRU and IRU noises on the spacecraft pointing stability, we must first derive the transfer functions from these sensor noises to the attitude estimator errors using the error propagation equations given above. The power spectral density of the spacecraft attitude error due to sensor noises could then be estimated. This sensor noise effect on S/C pointing instability, usually one of the largest contributors, could then be estimated. See the sub-section entitled "RWA Controller Error" for further details.

B. Star tracker bias

The SRU's NEA captures only effects due to photon noise, stray light noise, dark current noise, and readout noise. It does not capture SRU centroiding error, optical distortion, PSF (Point Spread Function) distortion, focal length scale error, and chromaticity. These bias account for the difference between the total measurement error of the SRU and its NEA. In this study, the specifications of the total measurement errors of the star tracker are 3.4 and 53 (twist) sêc, 3σ per axis.

C. Residual errors after in-flight calibrations

The inertial attitudes of the ACS axes are estimated by an attitude estimator. However, the pointing knowledge, control, and stability requirements are levied not with respect to the ACS frame but rather the SIM reference

frame. As such, the misalignments between these two coordinate frames, which vary from time to time, must be determined via periodic in-flight calibrations. Residual calibration error after an in-flight calibration is another error source that must be accounted for in the error budgets.

In a typical in-flight calibration, the "guide" interferometers are commanded to point in the direction of a pre-selected star field. The inertial attitude of the SIM reference frame could then be determined using the inertial attitudes of the captured guide stars. The inertial attitude of the ACS frame at the time when the guide stars are captured is available via time-tagged telemetry data of the attitude estimator. Using these two sets of attitude estimates, misalignment angles between the ACS and SIM coordinate frames could be determined. In general, the attitude estimation errors associated with the guide interferometers are significantly smaller than those determined by the ATE. Hence, the residual error after an in-flight calibration is approximated by the ATE error.

Before the first in-flight calibration, pointing of the guide interferometers will be affected by any structural misalignments between the ACS and SIM frames. These structural misalignments could come from the launch vibration, deployment of the collector pod arms, etc. The estimated "size" of this structural misalignment is on the order of 0.5-1° per axis. With an un-calibrated S/C pointing knowledge error that is this big, both angle tracking and fringe acquisition of the guide stars become difficult. To overcome this "start-up" problem, there might be a need to use the coarse acquisition camera of the guide interferometers to perform a spiral (or a mosaic) search around the expected locations of the guide stars. Also, the fringe acquisition time associated with the initial operations of the guide interferometers will be significantly longer than the nominal fringe acquisition time.

D. Thermal distortions between calibrations

In between in-flight ACS-to-SIM frame calibrations, thermal distortion of the precision structure (upon which both the SRU and the guide interferometers are mounted) generates additional pointing knowledge uncertainties that are not accounted for in the last in-flight calibration. Thermal distortion of the SRU mounting is controlled by imposing thermal stability requirement on the SRU itself. In this study, the per-axis thermal stability of the SRU is ≤ 4 sec (3σ) over any 30-day period. Implicit in this requirement is the need to perform an ACS-to-SIM frame calibration every 30 days.

Thermal distortion of the precision structure could be estimated as follows. Let α be the equivalent coefficient of thermal expansion of the precision structure material, $\Delta T/\Delta h$ be the temperature gradient across the surfaces of the structure, and L is a characteristic dimension of the structure. The thermal distortion of the structure could be approximated by: $2\beta_{thermal} = L/R = L \cdot \alpha \cdot \Delta T/\Delta h$, where R is the radius of curvature of the distorted structure. To control $\beta_{thermal}$, we impose bounds on both α and the maximum

allowable temperature excursion of the precision structure ΔT. In this study, we use α = 0.2 ppm per degrees C, and the precision structure is to be thermally controlled so that its temperature vary within ±2 °C throughout the five year mission time. One sec is allocated in the error budgets to account for these thermal distortions.

E. Slew-induced structural vibration

When a non-rigid S/C is slewed from one inertial attitude to another, residual structural vibration after the completion of the slew might not be insignificant. The magnitude of these residual vibration is related to both the natural frequencies and damping ratios of the major spacecraft structural modes. They are also related to the magnitude of angular acceleration used in slewing the S/C, as well as the elapsed time between the end of the slew and the time at which science observations is to begin (called settling time, T_s).

In Fig. 6, the SIM spacecraft is modeled by two rigid bodies connected by a spring-damper. One "rigid" body represents the precision structure while the second represents the solar array/sun shield (SA/SS). The equations of motion of the spacecraft are:

$$[I_{SC}+I_{SA}+m_{SA}(R+L)^2]\,\ddot{q}_1+[I_{SA}+m_{SA}(R+L)L]\,\ddot{q}_2 = T_{RWA} \quad (4)$$

$$[I_{SA}+m_{SA}(R+L)L]\,\ddot{q}_1+[I_{SA}+m_{SA}L^2]\,\ddot{q}_2 = -K\,q_2 - C\,\dot{q}_2$$

Here, I_{SC} is the moment of inertia of the spacecraft base-body and I_{SA} is the moment of inertia of the Solar Array/Sun Shield (SA/SS) (relative to its own center of mass). The angle q_1 is the angular displacement of the base-body with respect to an inertial frame, and the angle q_2 is the displacement of the SA/SS boom with respect to the base-body. T_{RWA} is the torque exerted on the base-body by the RWAs, and K and C are the spring stiffness and damping rate of the solar array boom. Dimensions R and L are defined in Fig. 6. The parameters K and C are related to the natural frequency (Ω) and damping ratio (β) of the first flexible mode of the structure: $K = \Omega^2\Delta$, and $C = 2\Omega\beta\Delta$, where $\Delta = m_{SA}[I_{SC}L^2+I_{SA}R^2]\div[I_{SC}+I_{SA}+m_{SA}(R+L)^2]$. Using these formulae, K and C could be selected to achieve a structural vibration mode with a 1-Hz frequency and a 1% damping ratio.

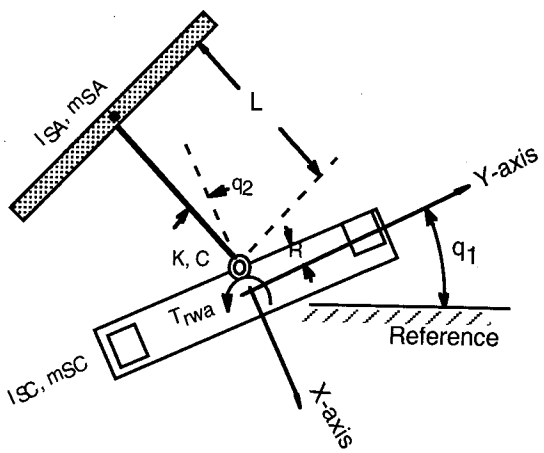

Fig. 6 A simplified two-dof SIM model

After a rest-to-rest slew, the residual rate and angle of the S/C are bounded by the following relations:

$$|\text{residual rate}| \leq \alpha_{slew} \cdot Q \cdot e^{-\beta\Omega T_s} \cdot \Omega^{-1} \text{ [rad/s]}$$

$$|\text{residual angle}| \quad \leq \alpha_{slew} \cdot Q \cdot e^{-\beta\Omega T_s} \cdot \Omega^{-2} \text{ [rad]}$$

Here, α_{slew} is the angular acceleration used in slewing the spacecraft, T_s is the settling time, and $Q = [I_{SA}+m_{SA}L(R+L)]^2 \div [m_{SA}(I_{SC}L^2+I_{SA}R^2)]$. Estimated inertia properties of the SIM spacecraft are:[1] m_{SA} = 400 kg, m_{SC} = 2600 kg, I_{SC} = 36,400 kg-m² (Z-axis), I_{SA} = 5,760 kg-m² (Z-axis), R = 1.5 m, and L = 5.9 m. Given $\Omega = 2\pi$ rad/s (1 Hz), β = 1%, $\alpha_{slew} = 5.24 \cdot 10^{-6}$ rad/s², and T_s = 1 minute. Using these numbers, the magnitudes of the residual rate and angle after a rest-to-rest spacecraft slew could be estimated.

F. RWA controller error

Pointing control of the SIM base-body is to be done using a set of four Reaction Wheel Assemblies (RWAs) for redundancy. A representative RWA attitude control loop is depicted in Fig. 7 [5].

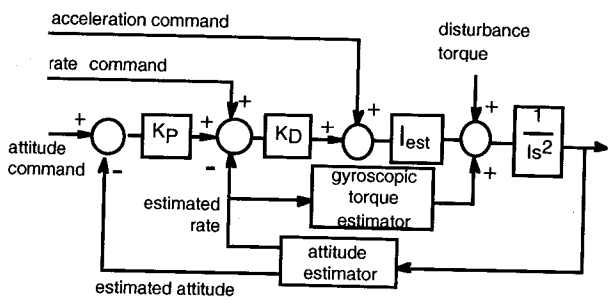

Fig. 7 A RWA controller design

In Fig. 7, K_P and K_D are the "proportional" and "derivative" gains of the RWA controller. It can be shown that $K_P \cdot K_D = (2\pi \cdot BW)^2$ where BW is the bandwidth of the RWA controller. In the presence of a persistent disturbance torque (T_D), a PD controller leads to non-zero controller error in the steady state. Its magnitude is given by: $T_D/\{(2\pi \cdot BW)^2 \cdot I\}$, where I is the moment of inertia of the affected S/C's axis. Here, controller error is defined as the difference between the commanded attitude vector and the ACS on-board estimate of the actual pointing vector. The approximate magnitude of per-axis solar radiation torque imparted on the S/C is $T_D \approx 5 \cdot 10^{-4}$ Nm. With an assumed controller bandwidth of 0.1 Hz, and $I = I_{min}$ = 4000 kg-m², the attitude controller error is less than 0.1 sec.

A mismatch in the gyroscopic terms used in the RWA controller could also lead to a steady-state controller error: $(\Delta I/I) \cdot (2\pi \cdot BW)^{-2} \cdot (I_{max}-I_{min}) \cdot \omega^2/I$. Here, $\Delta I/I$ is the percent knowledge error of the S/C's moment of inertia; I_{max} and I_{min} are the largest and smallest moments of inertia of the SIM spacecraft, respectively, and ω is the per-axis S/C rate. In this study, we use: $\Delta I/I$ = 10%, (I_{max},I_{min}) = (36000,4000) kg-m², and $\omega \leq 0.1$ °/s. An allocation of 3 sec is used in this study to account for attitude controller errors generated by the solar radiation torque and our imperfect knowledge of the S/C's inertia property.

To estimate the impact of the attitude estimator errors on the spacecraft pointing stability, via the RWA controller, we must once again refer to Fig. 7. In order to capture the effect of the structural flexibility in our estimation, we must replace the transfer function: S/C's angle/RWA's torque = $1/Is^2$ in Fig. 7 by a transfer function

$G(s) = q_I(s)/T_{RWA}(s)$ (where s is a Laplace variable) derived using the equations (4) and (5). In a quiescent state, the motion of the spacecraft θ is related to the estimated spacecraft attitude error (N_θ) and rate error (N_ω) by the following expression:

$$\theta(s) = -[K_P/\Delta(s)]\bullet N_\theta(s) - [1/\Delta(s)]\bullet N_\omega(s) \qquad (6)$$

where $\Delta(s) = s+K_P+\{I\bullet K_D\bullet G(s)\}^{-1}$. It can also be shown that the spacecraft attitude error (N_θ) and rate error (N_ω) are related to the imperfections of the SRU and IRU by the following approximate relations:

$$N_\theta(s)=[s/\vartheta(s)]\bullet N_1+[1/\vartheta(s)]\bullet N_2+[(sK_\theta+K_b)/\vartheta(s)]\bullet N_r \qquad (7)$$

$$N_\omega(s)=[s(s+K_\theta)/\vartheta(s)]\bullet N_1+[(s+K_\theta)/\vartheta(s)]\bullet N_2-[sK_b/\vartheta(s)]\bullet N_r \qquad (8)$$

The magnitudes of N_1 and N_2, the Power Spectral Density (PSD) of the angle random walk and bias stability of the IRU, respectively, are given in the sub-section entitled "Attitude Determination Errors". N_r is the squared NEA of the star tracker (the magnitude of the SRU's NEA was given in the same sub-section). The transfer function $\vartheta(s) = (s^2+K_\theta s+K_b)$, and K_θ and K_b are the Kalman-Bucy gains associated with the estimates of the spacecraft attitude and IRU bias, respectively. Using these expression, we can compute the power spectrum of the spacecraft motion, $B^2(f)$, using the specifications of the power spectral densities of the IRU and SRU noises. Finally, the spectrum of the S/C motion is frequency-weighted by $W_d(C)$ (where $C = 2\pi fT$ and T = window size in seconds) to determine the spacecraft pointing stability for time windows of various sizes. See also Fig. 8.

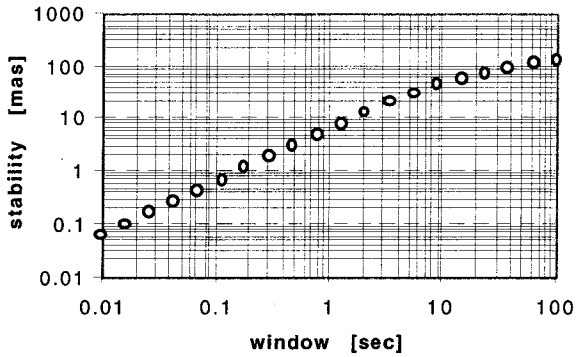

Fig. 8 Pointing jitter due to sensor noise

G. RWA-induced structural vibration

Since the specifications of the RWAs' cogging torque and torque ripple are negligibly small, only three RWA imbalances are considered in this study: dynamics imbalance, static imbalance, and axial run-out. If the spin axis of the RWA is its Z axis, then the dynamic imbalance of the RWA is defined as: $I_D = \{I^2_{ZX} + I^2_{ZY}\}^{1/2}$, where I_{ZX} and I_{ZY} denote the products of inertia's of the RWA in its X-Z and Y-Z planes, respectively. If the RWA is spinning at a rate of Ω_{rwa} rad/s, the dynamic imbalance generates a precessional disturbance torque with magnitude of $I_D\Omega^2_{rwa}$. The "total" disturbance torque T(t) generated by the dynamic imbalance of a RWA spinning at Ω_{rwa} rad/s could be approximated by [6]:

$$T(t) = \sum^N_{i=1} C^D_i\times\Omega^2_{rwa}\times\cos(h_i\times\Omega_{rwa}t+\phi^D_i) \qquad (9)$$

where harmonics h_i, i =1 to N are those that made significant contribution to T(t), and ϕ^D_i is the random phase angles between these harmonics. The parameters C^D_i are

amplitudes due to dynamic imbalance for the i^{th} harmonic. The coefficient for the fundamental harmonic is $C^D_1 = I_D$.

Instead of generating a disturbance torque, the static imbalance I_S of the RWA generates a precessional radial force. The RWA static imbalance is the product of the RWA's mass and its eccentricity. If the RWA is spinning at a rate of Ω_{rwa} rad/s, the static imbalance generates a force with magnitude of $I_S\Omega^2_{rwa}$. The resultant disturbance torque imparted on the S/C is then given by $d\times I_S\bullet\Omega^2_{rwa}$, where d is a representative moment arm. Obviously, the closer we can place the RWAs with respect to the S/C's c.m., the smaller is the impact of this disturbance force on the angular motion of the spacecraft. The run-outs (I_{RO}) of the RWAs produce an axial sinusoidal force that is also proportional to Ω^2_{rwa}. The disturbance force F(t) due to the RWA's static imbalance is:[6]

$$F(t) = \sum^N_{i=1} C^S_i\times\Omega^2_{rwa}\times\cos(h_i\times\Omega_{rwa}t+\phi^S_i) \qquad (10)$$

The disturbance force due to axial run-out is similar.

Since the disturbance torque and force generated by the RWAs' imperfections are all proportional to Ω^2_{rwa}, one obvious way to limit the impact of these imperfections on the S/C pointing performance is to bound the RWAs' rpms at time when stringent pointing stability must be maintained. In this study, a bound of ±1000 rpm is used. The implication of this RWA rpm bound is the possible need to unload the RWAs' momenta before times at which stringent S/C pointing stability must be met. Frequent RWA momentum unloadings add undesirable "ΔV" to the S/C which complicates S/C trajectory reconstruction. Settling times that must be allocated after these unloadings also impact the productivity of the SIM mission. A trade study between these two factors and the operational upper bound of the RWAs' rpm must therefore be made. To further attenuate the RWA-induced vibration on the S/C, the SIM's RWAs are to be mounted on vibration isolators. In this study, 15-Hz, 20% isolators are used.

Another RWA imperfection considered in this study is the RWAs' cogging torque. This torque varies sinusoidally as the RWA motor's pole pieces pass over the slots that contain the motor's field windings. That is, the cogging torque frequency is the product of the motor's frequency and the number of slots seen in one mechanical rotation of the rotor.

$$T_{cogging}(t) = T^P_{cogging}\times\sin(N_{slots}\times\Omega_{rwa}t) \qquad (11)$$

In this study, we assumed that the peak cogging torque ($T^P_{cogging}$) and the number of slots (N_{slots}) are 0.002 Nm and 18, respectively.

Yet another RWA imperfection is the commutation torque ripple (T_{ripple}) which varies sinusoidally as the brushless DC motor switches currents in the field windings. It is given by the following expression:

$$T_{ripple}(t) = \eta_{ripple}\times T^{command}(t)\times\sin(N_{phases}\times N_{poles}\times\Omega_{rwa}t) \qquad (12)$$

Here, η_{ripple} and $T^{command}(t)$ denote the ripple torque amplitude factor (8%) and the instantaneous commanded torque of the RWA, respectively. N_{phases} and N_{poles} denote

the number of motor phases (2) and poles (12), respectively. The samll cogging torque and torque ripple are neglected in the following calculations.

Fig. 9 depicts the orientations of the four RWAs with respect to the S/C's axes (with β =45° and ϕ =60°). With this configuration, the amplitude of the structural vibration induced by the RWAs, each with three sources of disturbance torque and forces could be estimated. Using the flexible S/C model described above (with $I_D = 9.1 \cdot 10^{-6}$ kg-m^2, $I_S = 3.6 \cdot 10^{-5}$ kg-m, $I_{RO} = 9.0 \cdot 10^{-5}$ kg-m, and d = 1 m), the 3σ amplitude of the RWA-induced vibration is less than 0.5 sec (all RWA rates $\leq$ 1000 rpm and with RWAs mounted on 15-Hz passive isolators).

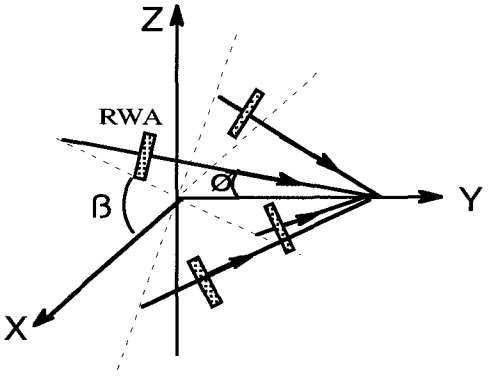

Fig. 9 Orientation of four RWAs

To estimate the impact of the RWA-induced disturbance torque's on the spacecraft pointing stability, we must first derive the transfer functions from the three disturbance sources to the spacecraft's angular motion using equations (4) and (5). The total disturbance spectrum of the spacecraft motion, $B^2(f)$, is then computed using the transfer functions and the power spectral densities of the RWAs' imperfections. The RWAs produce moments and forces with frequencies corresponding to several harmonics of the wheel speed. In this study, the Power Spectrum Densities (PSDs) are computed based on only six most significant harmonics of the RWA speed (1.0, 2.0, 2.82, 5.18, 5.60, and 7.50). The disturbance spectrum is next frequency-weighted by $W_d(C)$ (where $C = 2\pi fT$, T = 10 msec) to determine the spacecraft pointing stability for 10-msec time windows. The variation of RWA-induced spacecraft pointing stability with the size of the time window of interest is given in Fig. 10.

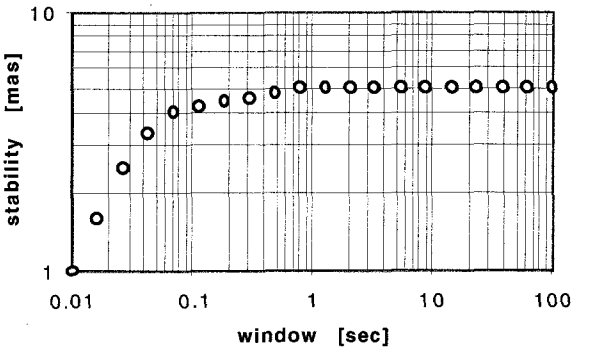

Fig. 10 Pointing jitter due to RWA imbalances

H. Spacecraft-Solar array control interaction

With reference to Fig. 1, the solar array/sun shield is attached to the spacecraft base-body via a solar array boom. The relative orientation of the boom with respect to the base-body is to be controlled via a 2-dof Solar Array Drive Mechanism (SADM). The solar array is to be controlled to within 1° of the Sun-line vector at all time in order to shield several base-body-mounted instruments from direct solar radiation.

To point the science interferometer at a new target star, we must slew the spacecraft in such a way that the solar array remains Sun-pointed throughout the slew. To this end, ACS must first compute two solar array articulation angles using knowledge of the inertial attitudes of both the target star and the Sun. These computed articulation angles are then sent as commands to a two-axis solar array control loop. The solar array is then articulated to its new position while the spacecraft is being slewed to its new inertial attitude. Once the new spacecraft orientation is achieved, the SA pointing loops are "disabled" (i.e., angle commands to stepper motors are set to zero). The SA boom is then held in position passively by both friction and the stepper motors' cogging torque (after they had been amplified by the harmonic drives). Without any control torque from the stepper motors, the spacecraft base-body will not experience any unwanted "reaction" torque (from the SA control loops) which might be detrimental to spacecraft pointing stability [8].

I. Thermal flutter

Thermal flutter on a spacecraft is most pronounced whenever there is a rapid heating rate change on one or more spacecraft structural members (e.g., its solar array or a flexible boom). Undesirable scenarios include spacecraft that makes frequent orbital eclipse transitions, and for a spin-stabilized spacecraft with a long flexible boom. None of these scenarios is applicable to SIM, which is a three-axis stabilized spacecraft in a Earth-trailing orbit. Nevertheless, an upper bound on the PSD of the SA-induced disturbance torque is established in this study as a way to limit the impact of thermal flutter on the pointing stability of the spacecraft base-body (see Fig. 11). As depicted in Fig. 11, we have assumed that most of the SA-induced disturbances are at or below 1 Hertz. That is, high frequency harmonics of the solar array (with frequency ≥ 10 Hz) are hardly excited by the 0.1-Hz bandwidth RWA controller. Details related to the SA design are not available at this time, and it is not possible to determine whether this PSD bound is achievable. Hence, Fig. 11 should be interpreted as an allocation or a target that we would require the SA design to achieve.

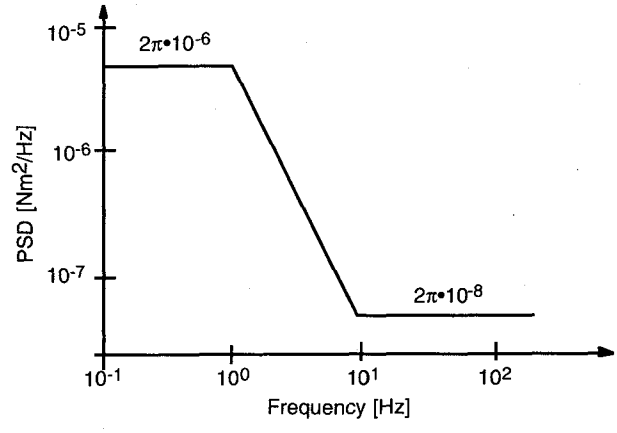

Fig. 11 PSD Bound of SA-induced torque

J. Spacecraft-instrument control interaction

For SIM to successfully perform an astrometric measurement, the Real-Time Control (RTC) subsystem of the interferometers must accomplish the following two tasks: (1) the pointing control loops must first acquire the target stars and then to keep them centered in the focal

plane of the fringe tracking cameras, and (2) the path-length control loop must first acquire a stellar fringe and then stabilize the fringe via continuous path-length adjustments. For further information on interferometer real-time control system, see Section I (Sub-section C) and [7].

Control torque generated by the actuators of the RTC control loops are "disturbance" torque to the S/C base-body control system. These torque must be bounded in order to limit their impact on the spacecraft pointing stability (see Fig. 12). In Fig. 12, we have assumed that most of the RTC-induced disturbances are at or below 10 Hertz, which is the assumed common closed-loop bandwidth of the pointing and path-length controllers.[7] Again, details related to the interferometer design are not available at this time, and it is not possible to determine whether this PSD bound is achievable.

One way to deal with the interactions between the RTC control loops and the spacecraft's attitude control loops is as follows: RTC control torque commands are feed-forward and sent to spacecraft attitude control system. The torque commands needed to perform spacecraft attitude control are augmented with the RTC control torque before they are sent to the spacecraft attitude control actuators (reaction wheels). This "feed-forward compensation" technique wasn't considered in this study.

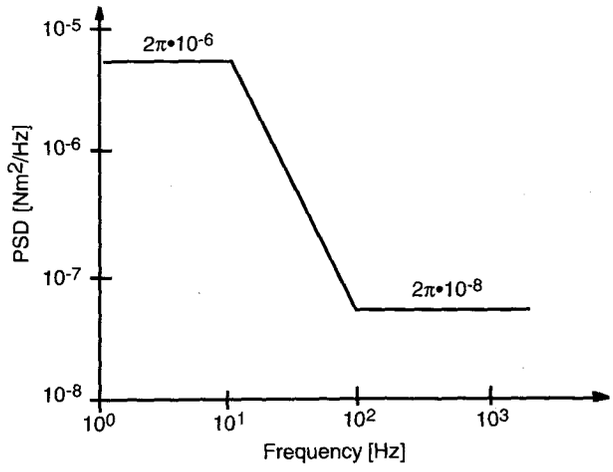

Fig. 12 PSD Bound of RTC-induced torque

Fig. 13 depicts how the weighted RMS pointing stability due to both the SA and the RTC system of the interferometers vary with the "size" of the time window of interest. Note that the two stability curves are almost on top of each other. That is, they impose equal "pain" to the enforcement of the spacecraft pointing stability requirement.

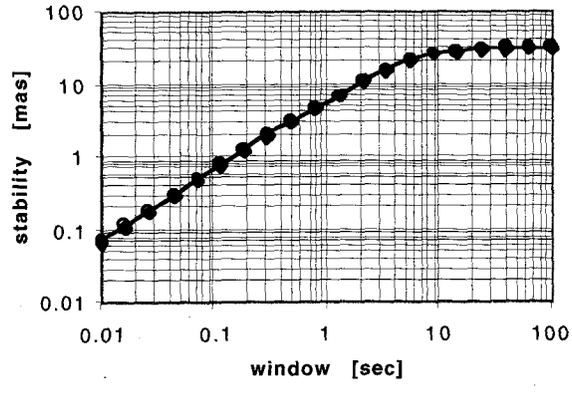

Fig. 13 Pointing jitter due to SA and RTC torque

V. PRELIMINARY ERROR BUDGETS

Preliminary error budgets for the SIM S/C pointing

requirements are given in this section. These error budgets are constructed to assess whether these requirements are achievable using COTS (Commercial-Off-The-Shelf) sensors and actuators. Methodologies described in Section IV are used to estimate the "sizes" of various error contributors. In Table 1, the component errors are root sum squared (RSS'ed) together to obtain the 3σ capability of the spacecraft pointing knowledge. The estimated overall capabilities are 7.3 and 66.8 sec about the S/C's X and Z, and Y axes, respectively. They are good margins between these per-axis capabilities and the corresponding requirements.

Table 2 is an error budget for the spacecraft pointing control requirements. In this error budget, we sum together various component errors (other than that of RWA controller error) to form a RSS (Root Sum Squares) sub-total. The overall spacecraft pointing capabilities are then determined by adding algebraically the RSS sub-total to the RWA controller error. The estimated overall pointing control capabilities are 10.3 and 69.8 sec about the S/C's X and Z, and Y axes, respectively. Again, we meet the requirements with good margins.

Table 3 is an error budget for the spacecraft pointing stability requirement. Again, the 1σ component errors are RSS'ed together to determine the 1σ capability of the spacecraft pointing stability. The estimated overall capability is ≈1.1 mas. There seems to be "enough" margin between the requirement and capability. However, one should keep in mind that our preliminary error budget did not include pointing stability errors due to high-frequency structural vibrations (that could not be captured by the 2-dof SIM model described above). Other transient disturbances, such as thermal snaps (thermal stresses that build up in the structure over time) are not captured in this preliminary study.

Table 1 Pointing Knowledge Error Budget

Error Sources	3σ per axis [sec]	
	X and Z axes	Y axis
Attitude determination error	0.3	2.1
SRU bias	3.1	47
Residual calibration error	3.2	47.1
SRU thermal mechanical instability	4	4
SIM frame thermal mechanical instability	0+	0+
Slew-induced structural vibration	0+	0+
RWA-induced structural vibration	0.5	0.5
SIM structural thermal distortion	1	1
Target command error	4	4
Per-axis capability	7.3	66.8
Per-axis requirement	20	120

Table 2 Pointing Control Error Budget

Error Sources	3σ per axis [sec] X and Z axes	Y axis
Attitude determination error	0.3	2.1
SRU bias	3.1	47
Residual calibration error	3.2	47.1
SRU thermal mechanical instability	4	4
SIM frame thermal mechanical instability	0+	0+
Slew-induced structural vibration	0+	0+
RWA-induced structural vibration	0.5	0.5
SIM structural thermal distortion	1	1
Target command error	4	4
Root-sum-squares	7.3	66.8
RWA controller error	3	3
Per-axis capability	10.3	69.8
Per-axis requirement	30	120

Table 3 Pointing Stability Error Budget

Error Sources	1σ per X and Z axes [mas]
Attitude determination and control:	
• Control error:	
Command resolution & timing jitter	0+
RWA speed reversals†	0+
• Attitude determination:	
IRU and SRU noise	0.1
Disturbances:	
• SA/SS drive mechanisms†	0+
• HGA drive mechanisms†	0+
• RWA-induced vibration	1.0
• Tape recorders (playback and rewind)†	0+
• interferometer control systems: angle and fringe tracking	0.1
Thermal-mechanical vibration:	
• Slew-induced vibration	0+
• Solar array thermal flutter	0.1
• Structure thermal instability	0+
Per-axis capability	≈1.1
Per-axis requirement	1.6

†Via careful sequence planning, these events are to be inhibited at times when tight pointing stability requirement must be met.

VI. POINTING STABILITY VERIFICATION CHALLENGES

The small "size" of the SIM S/C pointing stability requirement (1.6 mas) for small time "windows" presents several challenges in the end-to-end performance verification of that requirement.

As hinted in Section II, spacecraft jittery motions at frequencies higher than 44.2 Hz will have a greater impact on the spacecraft pointing stability (at 10-msec time windows) than motions below that frequency. If we are to verify this pointing stability requirement via time-domain simulations using a comprehensive model of the spacecraft system, we will face the following difficulty. Namely, it is usually difficult to model the high-frequency behavior of physical systems as well as to model their low-frequency behavior. This is true for structural dynamics, mechanisms

(such as break-away friction) that trigger high-frequency disturbances, and others. As such, the uncertainties associated with any analytical predictions of spacecraft small time-window pointing stability performance are likely to be large.

If we are to experimentally verify the 1.6-mas stability requirement, we must be able to measure jitter levels on the order of 0.2 mas. Assuming a signal-to-noise ratio of 10, a reliable jitter estimate could only be made if the contribution of all background noises is kept below 0.02 mas over frequency range of 80-120 Hz (1/10 msec = 100 Hz). To this end, it is of interest to know that a 0.02-mas noise floor at frequency range of 80-120 Hz is achievable [9]. We also note that many of the spacecraft's appendages such as its solar array/sun shield, etc. are not designed to deploy in the Earth's 1-g gravity field. As such, the SIM configuration used in these performance tests will deviate from that post-launch when the pointing stability requirement must be enforced. Also, the one-g loading on the RWA isolators must be off-loaded during these performance verification tests in order to allow the isolators to function properly in the tests. These and other challenges related to the verification of the spacecraft pointing stability performance are to be addressed in future phases of the SIM development program.

VII. CONCLUSIONS

Preliminary error budgets for the pointing knowledge, control, and stability of the SIM spacecraft are constructed using the specifications of commercial-off-the-shelf attitude determination sensors, attitude control actuators, and other spacecraft capabilities that had been demonstrated in past missions. These error budgets are constructed to assess whether these SIM S/C pointing requirements are reasonably achievable. Results obtained indicate that we can meet all the presently known spacecraft pointing requirements. Among all the pointing requirements considered, the pointing stability requirement is the most challenging.

A large number of derived requirements are generated from this study. Top on the list are specifications on attitude determination sensors and attitude control actuators. Other derived requirements include the minimum settling time after a rest-to-rest spacecraft slew, the minimum frequency and damping ratio of the first "N" modes of the solar array boom, the per-axis bandwidths of the RWA controllers, etc. Unless all these derived requirements are enforced, it will be hard to meet the required S/C pointing knowledge, control, and stability requirements.

Currently (fall, 1998), the SIM spacecraft configuration is still evolving. As such, spacecraft pointing requirements quoted in this study are likely to change with time. Moreover, we note that the common driver behind the three spacecraft pointing requirements stated in Section II was the need to acquire stars by the coarse acquisition camera and to acquire fringe by the fringe tracking camera.

However, once acquired, the stars must be tracked continuously by the angle pointing control loops (of both guide interferometers) to better than 30 mas, 1σ per axis [3]. Obviously, in order to achieve this level pointing control error for both interferometers (which are mounted on the precision structure of the SIM spacecraft), the motion of the spacecraft itself (over appropriate time windows) must be bounded! Yet no spacecraft pointing stability requirements are levied in Section II to support the tracking of the acquired stars. This and other "missing" spacecraft pointing stability requirements are currently being investigated and the current set of spacecraft pointing requirements will be augmented. Once defined, error budgets such as those given in Section V must be constructed in order to guide the design of the attitude control subsystem of the SIM spacecraft.

ACKNOWLEDGMENTS

The research described in this paper was carried out by the Jet Propulsion Laboratory, California Institute of Technology, and was sponsored by the National Aeronautics and Space Administration. The authors wish to thank K. Aaron, D. Bayard, R. Blue, G. M. Brown, C. Chu, P. Kobele, R. Laskin, G. Macala, J. Reimer, M. San Martin, L. Sievers, and G. Tsuyuki, their colleagues at the Jet Propulsion Laboratory, for many helpful discussions.

REFERENCES

[1] Aaron, K., Mateer, W.H., II, and Baron, R. L. (1998).

SIM Configuration Trades. SPIE Proceedings of the Astrometric Interferometry Conference, Kona, HI, March 20-24, 1998, pp. 714-19.

[2] Rayman, M. and Shao, M. (1992).

A Mission and System Design Option for the Orbiting Stellar Interferometer.

IAF-92-0527, 43rd International Astronautical Congress, Washington, D.C., August 28-September 5, 1992.

[3] Lucke, R.L., Sirlin, S.W., and San Martin, A.M. (1992).

New Definitions of Pointing Stability: AC and DC Effects.

The Journal of Astronautical Sciences, Vol. 40, No. 4, 1992, pp. 557-576.

[4] Danner, R. and Unwin, S. (1999).

Space Interferometry Mission - Taking the Measure of the Universe.

JPL 400-811, March 1999.

[5] Wong, E. and Breckenridge, W. (1995).

An Attitude Control Design for the Cassini Spacecraft.

Proceedings, AIAA Guidance, Navigation, and Control Conference, AIAA Paper 95-3274, August 1995, pp. 931-945.

[6] Masterson, R.A., Miller, D.W., and Grogan, R.L. (1999).

Development of Empirical and Analytical Reaction Wheel Disturbance Model.

Proceedings of the 40th AIAA/ASME/ASCE/AHS/ASC Structures, Structural Dynamics, and Materials Conference and Exhibit, St. Louis, MO, April 12-15, 1999 (AIAA Paper 99-1204).

[7] Bell, C.E., Walker, W.J., and Lee, A.Y. (1998).

Interferometer Real Time Control for the Space Interferometry Mission.

AIAA/IEEE 17th Avionics Systems Conference, Oct. 31-Nov. 6, 1998, pp. 335-47.

[8] Foster, C.L., Tinker, M.L., Nurre, G.S., and Till, W.A. (1995).

Solar-Array-Induced Disturbance of the Hubble Space Telescope Pointing System.

Journal of Spacecraft and Rockets, Vol. 32, No. 4, 1995, pp. 634-644.

[9] Blair, M.A. and Vadlamudi, N. (1988).

Jitter Performance Test for the Hubble Space Telescope: Methods and Results.

Proceedings of the 6th International Modal Analysis Conference, February 1-4, 1988, pp. 1682-90 (Editor: D.J. DeMichele, Society of Experimental Mechanics).

ABOUT THE AUTHORS

Dr. Allan Y. Lee received a Ph.D. in 1985 from Stanford University, Department of Aeronautics and Astronautics. In 1985-88, he was a staff research engineer with the Vehicle Systems Engineering department at General Motors Research Laboratories, Michigan. While at General Motors, he worked on various automobile control systems including an autonomous lane following vehicle. Dr. Lee is currently with the Avionics Systems Engineering Section of Jet Propulsion Laboratory. In 1995-97, he was the Cassini spacecraft attitude control subsystem Systems engineering team lead. He is now the project element manager of the attitude control subsystem of the Cassini spacecraft Operations team. At JPL, Dr. Lee has also contributed to Galileo mission to Jupiter, the Space Interferometry Mission, the Europa Orbiter mission, as well as the Variable Dynamic Test-bed Vehicle.

Dr. Jeffrey Yu is the instrument architect for the Space Interferometer Mission and a principal engineer at the Jet Propulsion Laboratory. He has worked on the design and implementation of space and ground based interferometers including the Palomar Testbed Interferometer, Keck Interferometer Array, and the DS-3 Separated Spacecraft Interferometer. Dr. Yu received a Ph.D. in Electrical Engineering from the California Institute of Technology. He has also been the deputy task manager for the interferometry technology program.

Peter B. Kahn joined the Jet Propulsion Laboratory as a member of the technical staff in February of 1987. He has been a System Engineer involved primarily in planetary flight projects including the Mars Observer Mission to Mars and the Cassini Mission to Saturn. Currently, he is the Flight System Engineer and System Engineering Element Manager on the Space Interferometry Mission. He has held this position since October 1996. Additionally, he is the Technical Group Supervisor for the Payload Development and Integration Group of the Flight Systems Section at JPL.

Dr. Richard L. Stoller received a Ph.D. degree in 1971 from Purdue University, School of Electrical Engineering majoring in Nonlinear Automatic Control and Estimation Theory. Since that time, Dr. Stoller has been at the Jet Propulsion Laboratory, Pasadena, California in Spacecraft System Engineering. He has held positions of staff system engineer, technical group supervisor, and operations team chief on the Voyager, Galileo, and SDIO Pathfinder projects. He led the system design for the Voyager Propulsion Module and, later, the Galileo Injection Module. He was the Spacecraft System Engineer for the Comet Rendezvous Asteroid Flyby (CRAF) project, and then became the spacecraft system engineer for the Cassini project. In 1999, he was project system engineer for the Space Interferometry Mission (SIM). Dr. Stoller received a NASA Exceptional Service medal for outstanding leadership and technical contributions.